NASA TECHNICAL NOTE

NASA TN D-2528

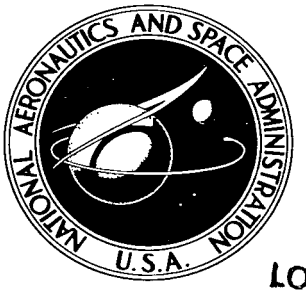

NASA TN D-2528

RADIOMETRIC OBSERVATIONS OF THE EARTH'S HORIZON FROM ALTITUDES BETWEEN 300 AND 600 KILOMETERS

by Thomas B. McKee, Ruth I. Whitman, and Charles D. Engle

Langley Research Center
Langley Station, Hampton, Va.

NATIONAL AERONAUTICS AND SPACE ADMINISTRATION • WASHINGTON, D. C. • DECEMBER 1964

RADIOMETRIC OBSERVATIONS OF THE EARTH'S HORIZON FROM ALTITUDES BETWEEN 300 AND 600 KILOMETERS

By Thomas B. McKee, Ruth I. Whitman,
and Charles D. Engle

Langley Research Center
Langley Station, Hampton, Va.

NATIONAL AERONAUTICS AND SPACE ADMINISTRATION

For sale by the Office of Technical Services, Department of Commerce,
Washington, D.C. 20230 -- Price $0.75

RADIOMETRIC OBSERVATIONS OF THE EARTH'S HORIZON FROM ALTITUDES BETWEEN 300 AND 600 KILOMETERS

By Thomas B. McKee, Ruth I. Whitman,
and Charles D. Engle
Langley Research Center

SUMMARY

Results from theoretical calculations and experimental measurements of sunlit horizons in the middle ultraviolet region (0.23μ to 0.29μ), the visible region (0.29μ to 1.0μ) and the near infrared region (0.75μ to 3.0μ) are presented. Experimental measurements are presented in the far infrared region (1.8μ to 25μ). The data were obtained with a four-channel radiometer which was flown on a Javelin rocket from the NASA Wallops Station.

Results indicate the horizons in the 0.75μ to 3.0μ spectral band are strongly affected by clouds. Horizons in the 0.29μ to 1.0μ spectral band are located at slightly higher altitudes than those of the 0.75μ to 3.0μ spectral band and for this measurement were probably produced principally by scattering.

In the 0.23μ to 0.29μ spectral band the horizons were at altitudes significantly higher than either those of 0.29μ to 1.0μ or 0.75μ to 3.0μ. These horizons were probably formed by scattering in the presence of atmospheric ozone. Theory predicts the peak of this ultraviolet horizon profile to be at approximately 58 km. The horizons measured in the 1.8μ to 25μ spectral band exhibited a wide variation which indicated an effective temperature difference. The extreme effective temperatures measured are 205° K and 270° K.

INTRODUCTION

Along with the capability of sending instruments and man above the atmosphere to make physical observations comes the necessity of determining the orientation and position of space vehicles. When a space vehicle is in the vicinity of the earth, the earth itself is a potential navigational aid. Determinable characteristic of the earth's apparent horizon such as thermal emissions of atmospheric constituents, the earth's thermal emission, scattered sunlight, or nonthermal atmospheric emissions could be used. Since the accuracy of determining orientation is dependent upon the stability and location of the physical characteristics to be utilized (as well as on the accuracy with which the measurement can be made and processed), it is desirable to make both theoretical calculations and experimental measurements of the earth's apparent horizon.

Measurements of the apparent horizon can also aid in studies of processes in the high atmosphere which may not be observable from the ground due to absorption in the atmosphere. As an instrument sensitive to radiant energy scans from space across the earth's horizon, a horizon gradient or profile is observed. For orientation purposes the ideal would be for the horizon profile to be invariant with sun position, meteorological conditions, geographic location, or solar activity.

This paper presents results of daytime horizon measurements in four broad spectral bands which extend from the middle ultraviolet to the far infrared: 0.23μ to 0.29μ, 0.29μ to 1.0μ, 0.75μ to 3.0μ, and 1.8μ to 25μ. The data were obtained with a four-channel radiometer which was flown on a Javelin rocket from the NASA Wallops Station. Part of the data presented in the present paper was previously discussed in reference 1.

SYMBOLS

A	clear aperture area of radiometer, cm^2
a	area of emitter in calibration, cm^2
f	focal length of calibration mirror, cm
G	optical gain produced by collecting mirror, dimensionless
g_λ	spectral transmission of filter in thermopile, dimensionless
H	effective irradiance on thermopile, W/cm^2
h	minimum altitude of line of sight, km
k	maximum detector responsivity, V/W
N	radiance, W/cm^2-sr
N_λ	spectral radiance, W/cm^2-sr-μ
P	effective power on detector, W
r	radius of earth, km
r_λ	spectral reflectivity of calibration mirror, dimensionless
T	temperature, ^oK
t_λ	spectral response of radiometer, dimensionless
V	signal voltage, V

λ wavelength, μ

ω field of view of radiometer, sr

Subscripts:

c calibration

λ wavelength

1 short wavelength limit of spectral band

2 long wavelength limit of spectral band

DISCUSSION

Energy Sources

A general discussion of the earth's apparent horizon can be separated according to energy sources. Three such sources are (1) scattered and reflected solar energy, (2) terrestrial and atmospheric thermal energy, and (3) other atmospheric emissions - that is, aurora and airglow. Since the spectral range of the measurements is from approximately 0.2μ to 25μ, the discussion of the horizon will be limited to that region. The solar energy curve approximates a blackbody that peaks at 0.46μ (fig. 1 and p. 16-15 of ref. 2) and has 99 percent of its energy occurring between 0.2μ and 3.9μ. The thermal emission of a 300° K blackbody is approximately equivalent to that of the earth, peaks at 9.7μ, and has 83.5 percent of its energy at wavelengths less than 25μ. From 0.2μ to 2μ the daylight horizon is principally due to solar energy. In the 2μ to 5μ region both sources can contribute to the horizon, and from 5μ to 25μ the horizon is due to terrestrial and atmospheric thermal energy. The aurora and airglow can cause horizons at various wavelengths which lie primarily between 0.2μ and 5μ. The distinction between aurora and airglow is nebulous and depends strongly upon the geographical location and the quantity or magnitudes of the emissions. Auroras are often defined as localized phenomena and as such do not have the stability or the predictability required in an application to horizon sensing; thus, only airglow is discussed in the present paper. The airglow lines discussed could be enhanced by auroral activity.

The first source of energy discussed is the solar energy that is scattered in the atmosphere and reflected from either clouds or the earth. Horizon gradients are produced by reflections and scattering. Since noctilucent clouds are localized and relatively rare, reflections from them are not considered. As a first approximation, scattering in that layer above the cloud and dust layer may be considered as Rayleigh and varies approximately with the inverse fourth power of wavelength. Reference 3 which discusses the radiance emerging from the top of a plane parallel atmosphere due to Rayleigh scattering shows the variation of radiance with optical path and solar orientation. In figure 1, curves are shown

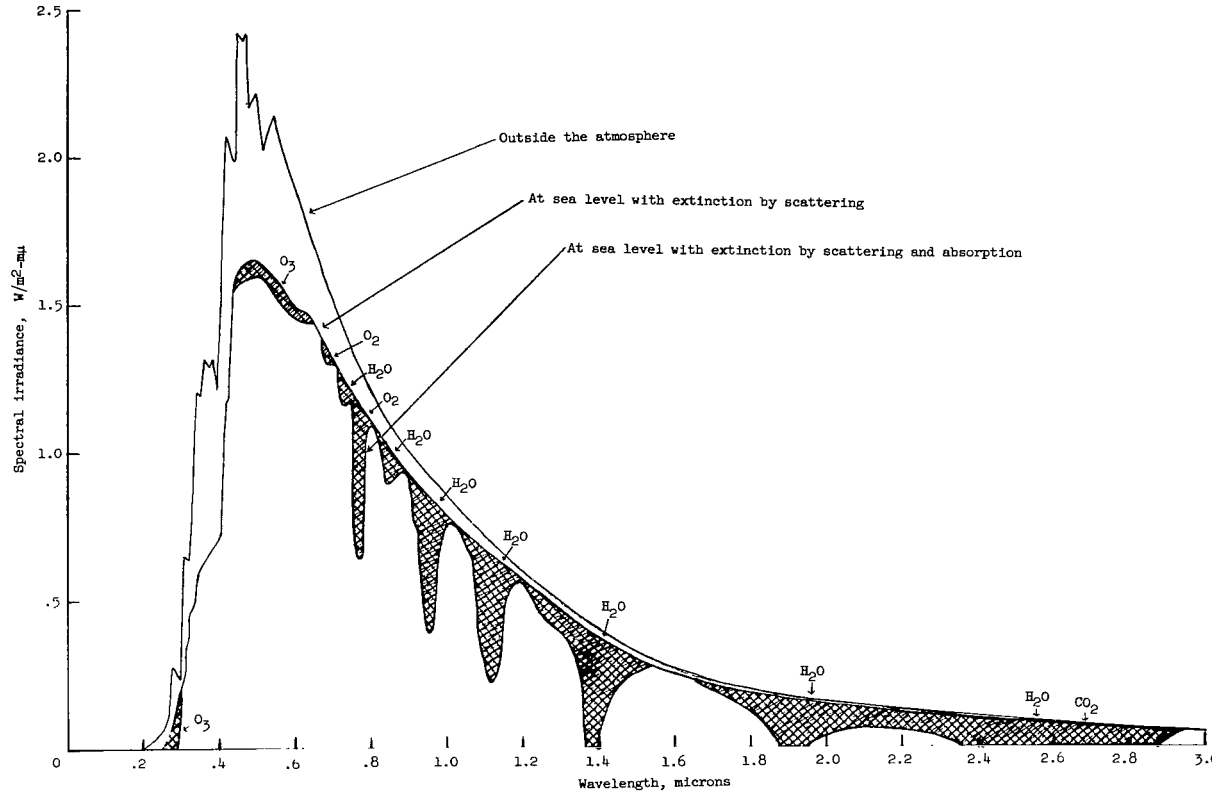

Figure 1.- Spectral energy curves related to the sun. (From ref. 2.)

for the solar spectral irradiances outside the atmosphere, at sea level with extinction by scattering, and at sea level with extinction by scattering and absorption. The amount of attenuation is a function of the total amount and vertical distribution of the absorbing component. The primary absorbing molecules are water vapor (H_2O), carbon dioxide (CO_2), and ozone (O_3).

The second source of energy is the thermal radiation from the earth and atmosphere. The earth radiates as a blackbody according to its temperature and this radiation is selectively absorbed by some of the constituents of the atmosphere. Part of the earth's thermal energy is lost directly to space and part is absorbed by the atmosphere that also emits thermal energy. Horizon gradients are formed by thermal radiation from the clouds, H_2O, CO_2, and O_3 in the atmosphere and the earth. Figure 2 shows the spectral distribution of energy emitted from a 300° K blackbody which is not unreasonable for the earth. Also shown are the spectral regions in which H_2O, CO_2, and O_3 are active. Water absorbs strongly in the region from 18μ to beyond 100μ and in a band centered at 6.5μ. Carbon dioxide has two important bands centered at 4.3μ and 15μ. Ozone has a rather narrow band centered at 9.6μ. The regions from 8μ to 9μ and 10.5μ to 12.5μ, having high transmission values, are called atmospheric windows. There are also a number of smaller windows between 1μ and 5μ. Discussions of radiative transfer and numerical data for the infrared are given in reference 4.

The third source of energy considered is the atmospheric emissions (airglow) that are not of thermal origin. (See ref. 5.) Since airglow is an excitation phenomenon of unique atoms or molecules, the altitudes which satisfy both the physical and chemical requirements for the emission of a unique wavelength form a narrow layer about the earth. The altitudes associated with airglow emissions are above those levels that are affected by ground weather conditions. The airglow emissions may show patchy structures that change with time. A horizon gradient formed by scanning through an airglow layer will be at a higher altitude and much smaller radiance than a scattering horizon. When the horizon is sunlit the radiance due to scattering may obscure the airglow emissions. Airglow has been studied primarily at night and at twilight because the scattered solar energy interfers with measurements made from the ground in the daytime. Recently, though, observations made from the ground of the day airglow have commenced since it is possible to distinguish day airglow from scattered energy by polarization characteristics. Scattered energy is polarized and airglow is unpolarized (ref. 6). Of the many spectral lines and bands that have been identified in the airglow only a few of the more intense ones are mentioned because the intensities from the airglow are very small. The most intense lines are the OI green line at 5577 Å, the OI red doublet at 6300 Å and 6364 Å, and the NaI doublet at 5890 Å and 5896 Å. The major band systems identified and the wavelength range of major energy emission are the Herzberg bands of O_2 (0.2μ to 0.5μ), the OH Meinel bands (0.5μ to 5.0μ), and the O_2 atmospheric bands (0.7μ to 0.9μ). Some of the night airglow emissions have already been identified in the day airglow and all of the night airglow emissions should be present in the day airglow even though their intensities could be either enhanced or diminished dependent upon their production mechanism.

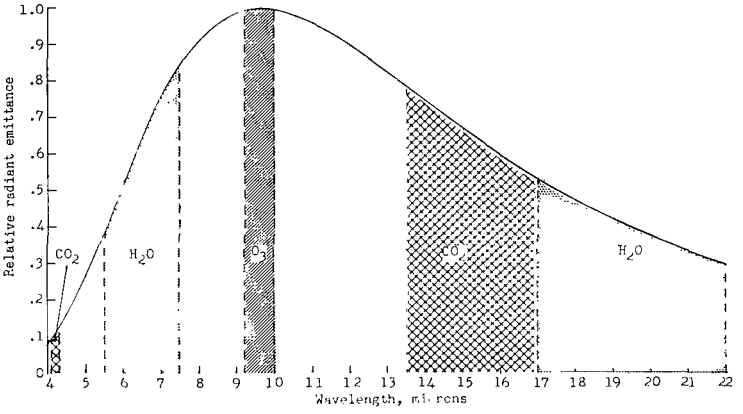

Figure 2.- Spectral shape of 300° K blackbody with approximate absorption regions of H_2O, CO_2, and O_3.

Predicted Horizons

Some horizon properties can be predicted for the spectral bands which were measured in this experiment. These spectral bands were 0.23μ to 0.29μ, 0.29μ to 1.0μ, 0.75μ to 3.0μ, and 1.8μ to 25μ. As an instrument scans from space to earth, the instrument's line of sight must instantaneously have a minimum altitude. Figure 3 shows the geometry of a conical scan. The earth has a radius r, and an individual line of sight passes the earth at a minimum altitude h.

Scattering and airglow can produce horizons, or limbs, in the 0.23μ to 0.29μ spectral band of the ultraviolet. Airglow due to the Herzberg bands of O_2 has been detected at an altitude of approximately 90 km by rocket-borne instrumentation at night (ref. 7). Scattering produces limbs at lower altitudes. In this spectral band little solar energy reaches the earth because of absorption by ozone O_3. The absorbed solar energy causes a rise in temperature in the ozone layer instead of an immediate reemission. The calculated radiance of the atmosphere due to primary Rayleigh scattering in the presence of O_3 is given in reference 8. In figure 13 of reference 8, theoretical limbs in the band from 0.22μ to 0.29μ are shown for these conditions: vehicle azimuth, 101.5°; vehicle zenith, 20°; sun azimuth, 171.2°; sun zenith, 57.15°; vehicle attitude, 450 km; and look angle, 65°. The theoretical limb, including absorption due to ozone, from figure 13 of reference 8 is reproduced in figure 4. The geometric conditions for this theoretical profile are similar to those encountered in flight; therefore, the profiles have been designated northern and southern horizon accordingly. (See fig. 3.) The magnitude and altitude of the peak radiances are functions of the total amount and vertical distribution of O_3 as well as the geometric conditions (ref. 8). These theoretical limb profiles had maximum radiance at approximately 58 km, and the difference in peak radiance between the northern and southern horizon was due primarily to sun orientation.

A limb profile, in the spectral region from 0.22μ to 0.29μ, that exhibits a definite peak should be useful for horizon definition because the peak occurs at a high enough altitude to be unaffected by meteorological conditions in the low atmosphere. The altitude variations of the peak radiance due to O_3 variations are not known. Measurements reported in reference 9 indicate no measurable radiances exist at night in this spectral region, but the instrument was not sensitive enough to respond to night airglow.

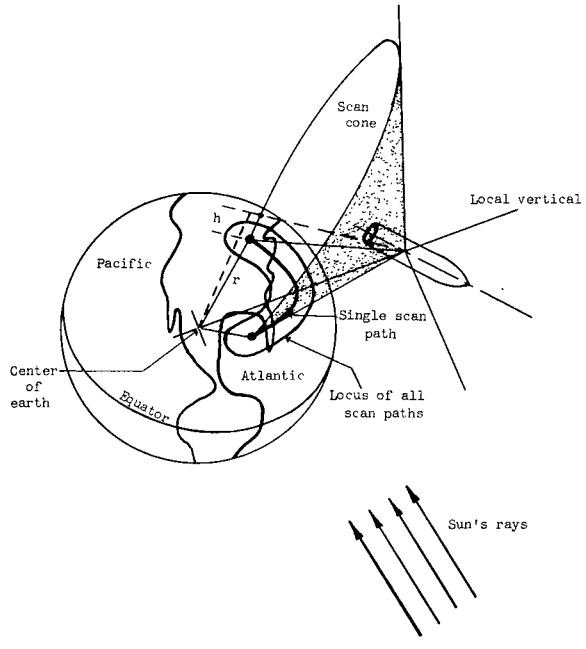

Figure 3.- Flight geometry.

In the spectral band from 0.29μ to 1.0μ, both airglow emissions and scattering cause horizon profiles. Airglow produces a horizon at higher altitude than the scattering but on a sunlit limb the radiance due to scattering is much larger than the radiance due to airglow. A theoretical horizon profile due to primary Rayleigh scattering with no absorption has been computed for the band from 0.29μ to 1.0μ by using equations from reference 8 and the same geometry conditions as used previously for figure 4; this profile is presented in figure 5. The curve shows a rapidly increasing radiance with decreasing altitude until 15 km where the slope starts to change and a plateau is reached by 7 km. Since clouds occur at altitudes greater than 10 km, this profile could be affected by local weather conditions. The difference in the radiance between the northern horizon and southern horizon is primarily due to the sun's position.

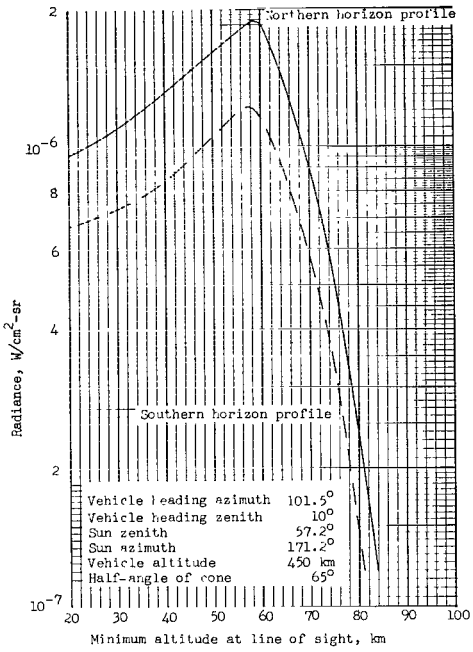

Figure 4.- Theoretical horizon profile for primary Rayleigh scattering with absorption by ozone in spectral band from 0.22μ to 0.29μ.

In the band from 0.75μ to 3.0μ, the absorption by H_2O and CO_2 causes the spectral shape of the radiation from the horizon to differ considerably from that of the sun's emission. Airglow emission from OH is very strong in this region but does not approach that of reflected sunlight. A theoretical horizon profile in the region from 0.75μ to 3.0μ for primary Rayleigh scattering is shown in figure 6. (Geometric conditions used in the calculation are the same as those previously discussed.) The absorption due to H_2O, O_2, and CO_2 occurring in this band is not included in this calculation. Since the scattering profile shows no peak or plateau above 5 km, the termination of the profile would be caused by reflections from the earth or clouds; therefore, the horizon would undoubtedly be dependent on cloud conditions.

In the band from 1.8μ to 25μ, the horizon would be caused primarily by emission of H_2O, CO_2, O_3, and the earth since the sun and airglow effects are minimal for wavelengths greater than 6μ. Computed horizon profiles due to thermal radiation for the 6.5μ H_2O band, 9.6μ O_3 band, 10.75μ to 11.75μ window, 15μ CO_2 band, and the rotational water band (21μ to 125μ) were reported in reference 10. The authors of reference 10 conclude that the 15μ CO_2 band and the 21μ to 125μ water region are the most promising wavelength regions to find a stable horizon for horizon sensing. The 6.5μ H_2O band and atmospheric window regions are variable and they depend on water content and cloud conditions. In reference 11 a criterion for horizon scanner system performance is developed, and with the use of existing theoretical horizon profiles the author of reference 11 concludes that the 15μ CO_2 band is the best region for horizon definition. The band from 1.8μ to 25μ used in the present investigation is dependent on clouds and water content of the atmosphere.

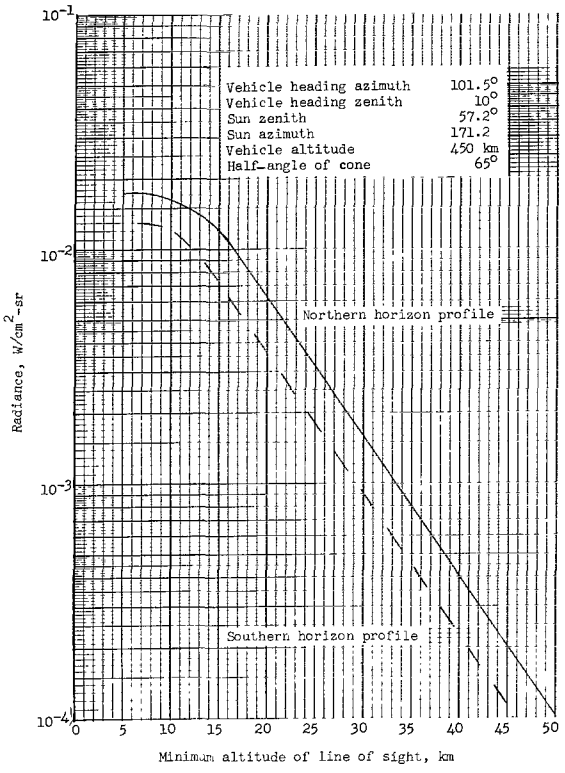

Figure 5.- Theoretical horizon profile for primary Rayleigh scattering in spectral band from 0.29μ to 1.0μ, assuming no absorption.

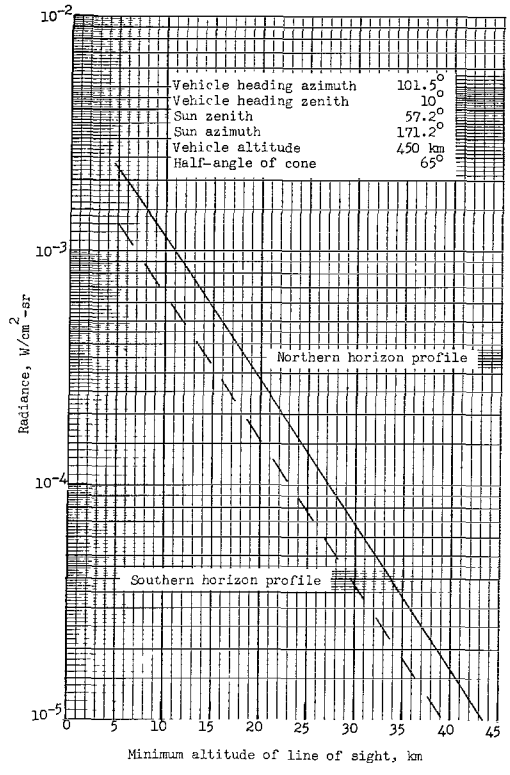

Figure 6.- Theoretical horizon profile for primary Rayleigh scattering in spectral band from 0.75μ to 3.0μ, assuming no absorption.

EXPERIMENTAL PROCEDURE

A four-channel radiometer flown as a payload on a four-stage Javelin rocket was launched from NASA Wallops Station on November 17, 1961, at 11:06 a.m. EST. The vehicle was spin stabilized at 600 rpm and then a yo-yo type despin system was used to reduce the spin rate for the experiment. Despin was not successful, and a residual spin of 400 rpm resulted instead of the desired rate of 40 rpm. Spin rate decreased steadily from 400 rpm to 300 rpm in a period of 240 seconds. Horizons were observed from vehicle altitudes under 300 km to a peak of 610 km.

Geometry for the experiment is illustrated in figure 3. The optical axis of the radiometer was fixed at 65° with respect to the rear of the rocket. As the rocket spun, the lines of sight of the radiometer formed elements of a cone; thus, the scan geometry is the intersection of a cone and a sphere in which approximately half of the cone actually intersects the sphere. The attitude (angle between spin axis and local horizontal) of the rocket was between 78° and 84° during the time the horizons were observed. Attitude was determined from the geometry by using the radius of the earth, half-angle of the cone, altitude of the rocket (radar), and the fraction of a roll cycle for which the radiometer

viewed the earth. The actual data then showed the radiometer looking at space, horizon, earth, horizon, and space in a cyclic fashion.

Instrumentation

The instrument package which was attached directly to the fourth-stage rocket motor carried the four-channel radiometer and its support equipment plus instruments to determine the performance of the vehicle. Figure 7 shows the instrument section just prior to installation on the rocket motor. The four channels of the radiometer are optically alined.

As an optical instrument the radiometer is a simple unsophisticated light-collecting device. Radiometer characteristics are given in table I. Optical structure of the radiometer is illustrated in figure 8. Figure 8(a) shows the construction for the near infrared (NIR), visible (VIS), and far infrared (FIR) channels. Light enters

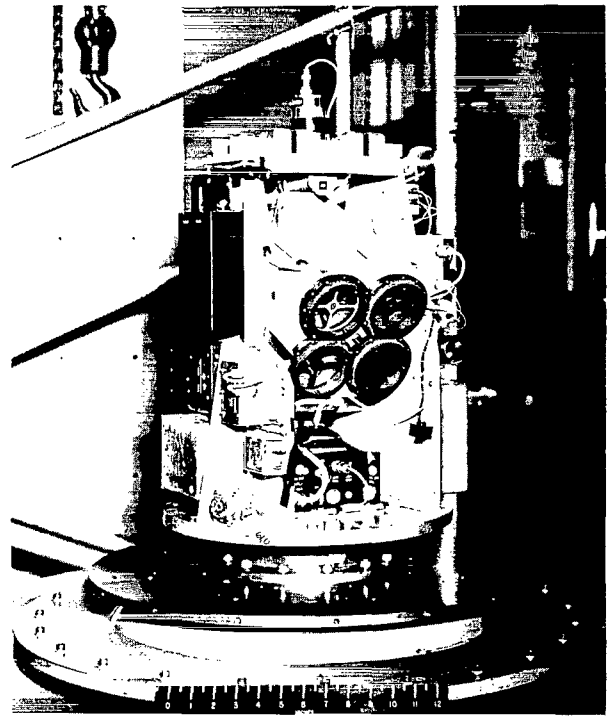

L-61-8243
Figure 7.- Photograph of instrument section.

TABLE I.- RADIOMETER CHARACTERISTICS

	UV	VIS	NIR	FIR
Spectral band	0.23μ to 0.29μ	0.29μ to 1.0μ	0.75μ to 3.0μ	1.8μ to 25μ
Focal length	25.4 cm	25.4 cm	25.4 cm	7.60 cm
Aperture	7.60-cm diameter	7.60-cm diameter	7.60-cm diameter	7.60-cm diameter
Detector	Photomultiplier	PbS (1 mm by 1 mm)	PbS (1 mm by 1 mm)	Thermistor bolometer (1 mm by 1 mm)
Filter	Composite filter[1]	Color filter (2.54 mm)	Color filter (2.54 mm)	Germanium (1 mm)
Channel time constant	<0.0003 sec	<0.0003 sec	<0.0003 sec	0.001 sec
Field of view	0.22° by 0.22°	0.22° by 0.22°	0.22° by 0.22°	0.75° by 0.75°

[1]Contains $NiSO_4.6H_2O$ (8 mm), Polyvinyl alcohol incorporating cation X, UV transmitting color filter (3 mm), and quartz (6 mm). (See ref. 12.)

the aperture, is reflected by the parabolic mirror, and is focused on the detector which is located at the focal point and supported by a spider (fig. 7). One leg of each spider serves as a conduit for necessary electrical connections. A thermistor to measure the operating temperature of the detector is also located on the spider. For the NIR, VIS, and FIR the detector dimensions and the focal lengths define the field of view. Optical filters for NIR and VIS are placed at the aperture whereas the FIR has a filter attached to the detector. Figure 8(b) shows the middle ultraviolet (UV) channel which has a 45° flat mirror held in the converging beam which reflects the light through a field stop at the focal point and then onto the detector. An optical filter is placed between the field stop and the detector. A quartz window is also placed in the aperture to help provide a seal for the nose section which is pressurized. A larger field of view was necessary in the FIR than in the NIR, VIS, and UV in order that sufficient energy could be obtained for recording purposes. Transmissions of the optical filters are shown in figure 9. A filter similar to the composite filter is discussed in reference 12. Typical spectral responses of the detectors are indicated in figure 10.

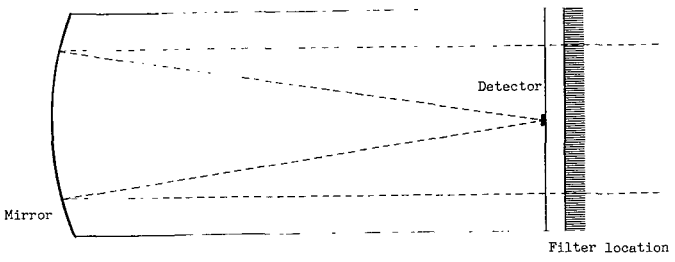

(a) NIR, VIS, and FIR channels.

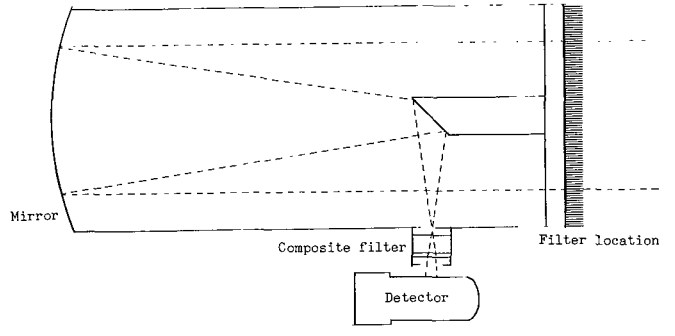

(b) UV channel.

Figure 8.- Optical system.

The FIR channel employed an AC amplifier which had sufficient high frequency response to reproduce the required signal, but had insufficient low frequency response to maintain the signal without droop. The UV, NIR, and VIS channels were directly coupled and, thus, capable of providing a signal without droop.

The telemeter system used was a standard FM-FM system in which a voltage input is converted to a frequency by a voltage oscillator; eight channels of telemetry were used. The four radiometer and three accelerometer channels were telemetered continuously while the remaining channel was commutated between the four thermistors used to measure the temperature of each detector. Each thermistor was sampled 2.4 times per second.

Calibration

The object of the calibration was to relate the received telemetry signals to radiances measured in flight. In this section the methods used to calibrate the FIR and VIS channels are discussed. Because of conditions peculiar to the UV and NIR channels, sufficient confidence in the absolute radiances was not attained; consequently, only relative radiances are presented. A general

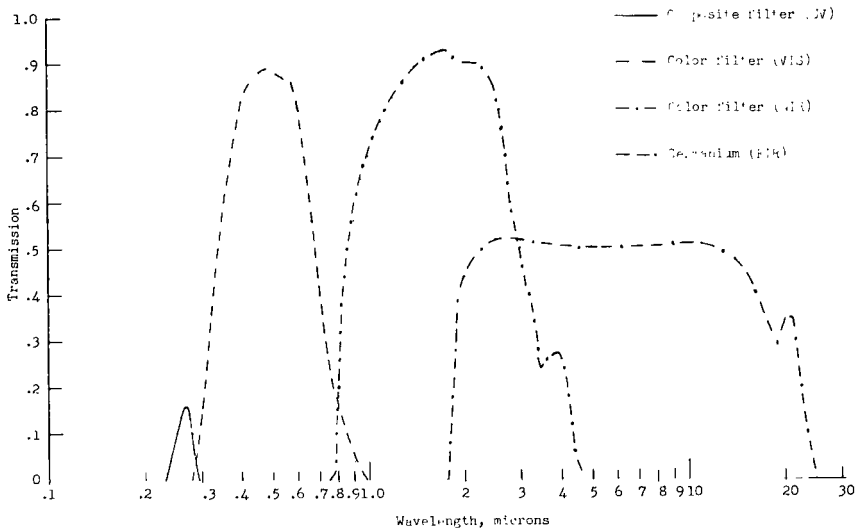

Figure 9.- Transmission of optical filters.

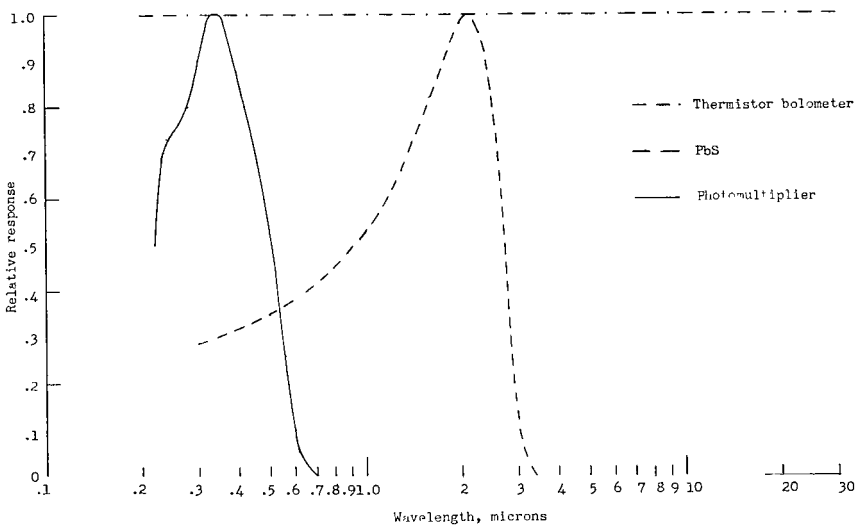

Figure 10.- Relative spectral response of detectors.

discussion of calibration procedures, apparatus, and problems is given in reference 13. Since sources were not large enough to fill the field of view and to be focused on the detector at the focal point, the calibration sources were optically moved to infinity by placing them at the focal point of a parabolic mirror. The radiometer was placed in the resulting parallel beam, and the image size was smaller than the detecting elements. Figure 11 illustrates the optical setup for calibration. The calibration source was placed as close to the optical axis of the calibration mirror as possible without interfering with the radiometer. A collecting mirror was placed in front of the radiometer. This mirror collected energy in the parallel beam onto a thermopile for measuring the irradiance at the aperture of the radiometer because the thermopile

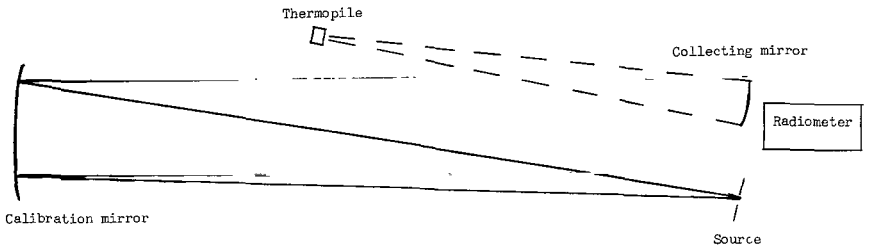

Figure 11.- Sketch of optical system for calibration.

was not sensitive enough to measure directly the irradiance of the beam. The thermopile was calibrated by the manufacturer using a standard carbon lamp. The quartz window of the thermopile transmitted radiation from 0.2μ to 4.5μ. The second mirror was removed after the measurement with the thermopile was made.

Radiant energy from the calibration mirror and the background around the calibration source could contribute to the parallel beam and thus to the radiometer output. This radiation is thermal in origin and of about 300° K since that was approximately the temperature of the darkened room during calibration. There was not enough energy to cause noticeable error in the VIS channel; the FIR calibration source was chopped and only the change in energy was measured.

The object of the flight measurement was to determine the radiance within a spectral band which was

$$N = \int_{\lambda_1}^{\lambda_2} N_\lambda \, d\lambda \tag{1}$$

During flight the effective power on the detector when the field of view was filled was

$$P = A\omega \int_{\lambda_1}^{\lambda_2} N_\lambda t_\lambda \, d\lambda \tag{2}$$

The resulting voltage was

$$V = kP = kA\omega \int_{\lambda_1}^{\lambda_2} N_\lambda t_\lambda \, d\lambda \tag{3}$$

where k is not necessarily constant for all values of P.

During calibration the effective power and voltage were

$$P_c = \frac{a}{f^2} A \int_{\lambda_1}^{\lambda_2} N_{c,\lambda} t_\lambda r_\lambda \, d\lambda \tag{4}$$

$$V_c = k_c P_c = k_c \frac{a}{f^2} \int_{\lambda_1}^{\lambda_2} N_{c,\lambda} t_\lambda r_\lambda \, d\lambda \tag{5}$$

The FIR channel was calibrated by using a blackbody at 1273° K; thus, $N_{c,\lambda}(T,\lambda)$ was known. Variations in irradiance at the radiometer aperture were accomplished by changing the emitting area of the blackbody. In equation (4), a, A, f, and r_λ were measured. The spectral response of the radiometer t_λ was formed by the product of the characteristics of the radiometer filter, mirror, and detector. Effective power P_c was computed from equation (4) and V_c was measured. From these data, a curve of P_c as a function of V_c was drawn. Since the same detector and electronics were used in flight and calibration, $k = k_c$ and $P = P_c$. Thus, a curve for P_c against V_c is the same as a curve for P against V. Next the assumption was made that in the flight measurement the radiometer viewed a blackbody $N_\lambda(T,\lambda)$ of temperature T. For each value of T there is a value of P (eq. (2)) and, consequently, one for V. A curve for T against V was drawn. The radiance was determined by integrating N_λ for λ_1 to λ_2 for a particular temperature.

A tungsten lamp was used to calibrate the VIS channel. Color temperature of the lamp was determined with an optical pyrometer to be 3072° K. The lamp was placed in a box with a blower for cooling and radiated through a 0.318-cm-diameter hole for a source area. Variations were made in the beam irradiance by placing different combinations of neutral density filters in front of the lamp aperture. Consequently, the symbol a in equation (4) is actually the area of the aperture times the transmission of the neutral density filter which was considered a constant over the wavelength region of interest. In equation (4) all terms are known except $N_{c,\lambda}$, but the normalized shape of $N_{c,\lambda}$ is known; the absolute values of $N_{c,\lambda}$ may be determined with the aid of a measurement.

The irradiance measured by use of a thermopile placed in the converging beam of the collecting mirror which introduced an optical gain of G (fig. 11) was

$$H = \frac{a}{f^2} G \int_{\lambda_1}^{\lambda_2} N_{c,\lambda} r_\lambda g_\lambda \, d\lambda \tag{6}$$

Since H, a, f, G, r_λ, and g_λ were measured and the spectral shape of $N_{c,\lambda}$ was known, the absolute values of $N_{c,\lambda}$ may be determined with the aid of a graphical integration.

The absolute $N_{c,\lambda}$ was next used to evaluate equation (4) for P_c. From these data a curve for P_c as a function of V_c was drawn. Again $P_c = P$ and $V_c = V$. Finally, a spectral shape was assumed for N_λ in equation (2). A spectral shape equivalent to that of a 5800° K blackbody was chosen. In a manner identical to that used to evaluate equation (7) for $N_{c,\lambda}$, equation (3) may be evaluated for N_λ for each value of P. Upon the integration of N_λ

between λ_1 and λ_2 a curve of N as a function of V was drawn which was the final calibration curve.

PRESENTATION OF DATA

The vehicle flew in an easterly direction from the NASA Wallops Station and rolled in such a manner that the fields of view swept onto the earth in the vicinity of the Gulf of Mexico, swept out across the Atlantic Ocean, and then off the earth near the Great Lakes and Hudson Bay. For convenience the gradients occurring while going onto the earth will henceforth be called southern horizons and those occurring while going from earth to space will be called northern horizons. Figure 12 shows the area in which the scans occurred, the areas in which all horizon regions occurred, and the ground-based observations for the cloud cover conditions in that area. As previously stated, theory indicates that local cloud conditions at the horizon can affect the gradients in the NIR and VIS channels. Consequently, a knowledge of cloud cover aids in the interpretation of the data.

Flight Records

Any change in horizon radiance due to increased rocket altitudes was completely obscured by the changes in horizon radiances caused by observing different geographical locations on the earth from approximately the same rocket altitude. Shown in figure 13 are typical flight records chosen to illustrate pertinent features. At the top of these records is a coded time signal with a time response of 1000 cps. Immediately below the time signal is an accelerometer channel, then the four data channels. The NIR and VIS channels displayed similar characteristics during the on-earth portion of the scan; this is not unexpected since the spectral regions overlap and the optical depths of the atmosphere in these regions are low enough to make reflections from the earth's surface and from clouds dominate the outcoming radiance. The vertical line in figure 13(a) is drawn to point out one of the many instances when peaks in the NIR and VIS were in near coincidence with a peak in the UV and a dip in the FIR. This was quite standard but in other examples the UV and FIR responses would shift in relationship to the NIR and VIS peaks indicating that the phenomenon did not have the same shape in all the spectral bands or that the integrated effect due to the different size of view in the FIR channel could result in a displacement of the maximum indicated energy change. The on-earth peak in the NIR, VIS, and UV regions are due to reflection instead of scattering phenomena. In the FIR channel the signal decrease was probably caused by a highly reflective cloud or earth surface that was also cold. Signal changes occurring during the on-earth portion of the scan in the NIR, VIS, and FIR channels were competitive with the horizon gradient; this was not true in the UV channel. In the UV channel at no time was the signal below 20 percent of the maximum radiance but in the VIS channel the signal approached 10 percent of maximum amplitude at times and in the NIR channel the signal approached the noise level. These values indicate that there were steeper gradients and larger changes in magnitude in the VIS and NIR channels than in the UV channel and that there was most variability in signal strength in the NIR channel and least in the UV channel. As the radiometer approaches the horizon from space the UV channel is the first to respond then,

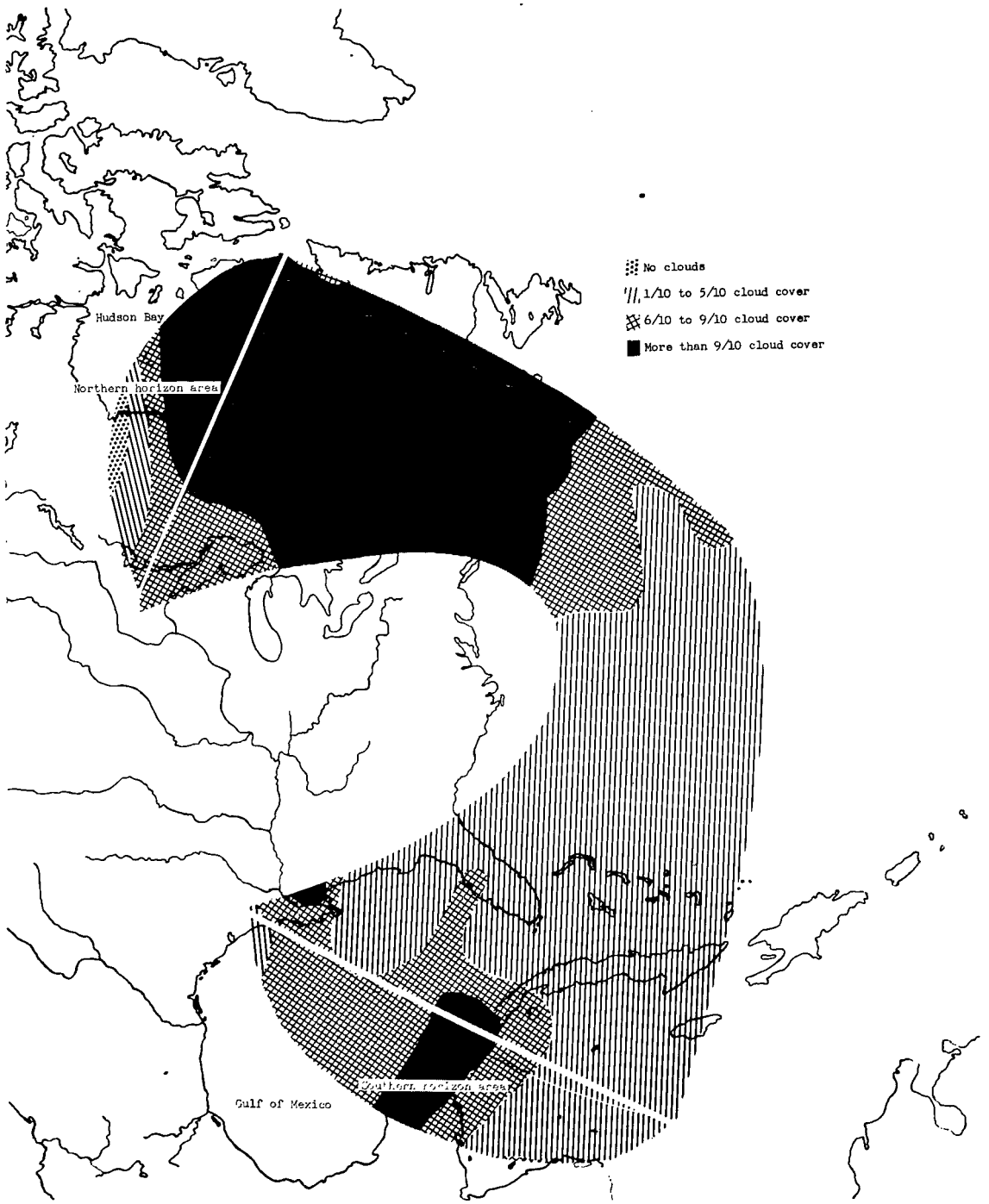

Figure 12.- Summation of total cloud cover in scanned regions.

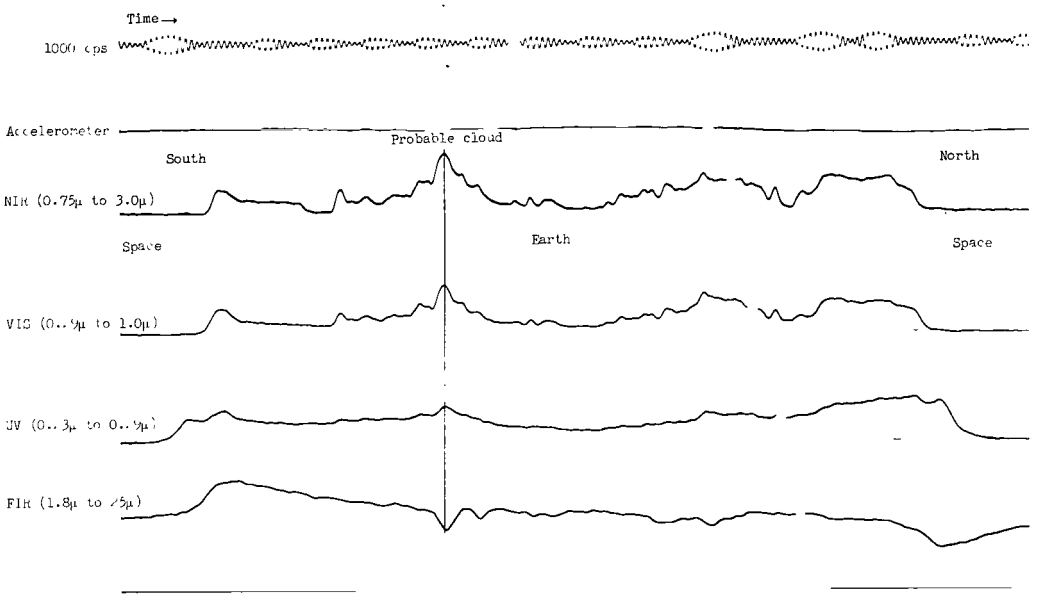

(a) Vehicle altitude of 300 km.

Figure 13.- Samples of telemeter record.

in order, the FIR, VIS, and VIR channels. When scanning from earth to space the responses terminate in the reverse order. Since the field of view of the FIR channel was so much larger than that of the other three channels, it was impossible to attach a significance to its relative location. It was possible to read the time difference between any two events to within 0.0005 sec. Errors in the relative alinement of the radiometers could produce time errors no greater than 0.001 sec. The time differences between the initial responses of the UV, VIS, and NIR channels were always greater than 0.001 sec indicating that the UV channel responded to an energy source higher in the atmosphere than did the VIS channel and it in turn responded to an energy level at a higher altitude than the NIR channel. In practically every instance after the initial gradient in the UV channel had been completed a second gradient nearly coincident with the VIS response occurred. The data showed that there was a different effective diameter of the earth in the UV channel than there was in the NIR channel or VIS channel.

The FIR radiation was not chopped even though the FIR channel was AC coupled so radiance changes were recorded accurately, but the signals for regions of non-varying or slowly varying radiance levels could not be held. The frequency response of the AC coupled circuit allowed a slowly varying signal to decay toward the reference voltage level. The high spin rate coupled with the slow decay in the amplifier due to previous signal variations resulted in northern horizon gradients occurring while the amplifier was decaying. This decaying signal enhanced the difficulty of determining where the horizon gradients started. The signal decay in the FIR channel is most obvious immediately after the southern horizon. (See fig. 13(c).)

Differences in signal level and gradient definition at the same altitude are observed. (Compare fig. 13(b) with 13(c) and fig. 13(d) with 13(e).)

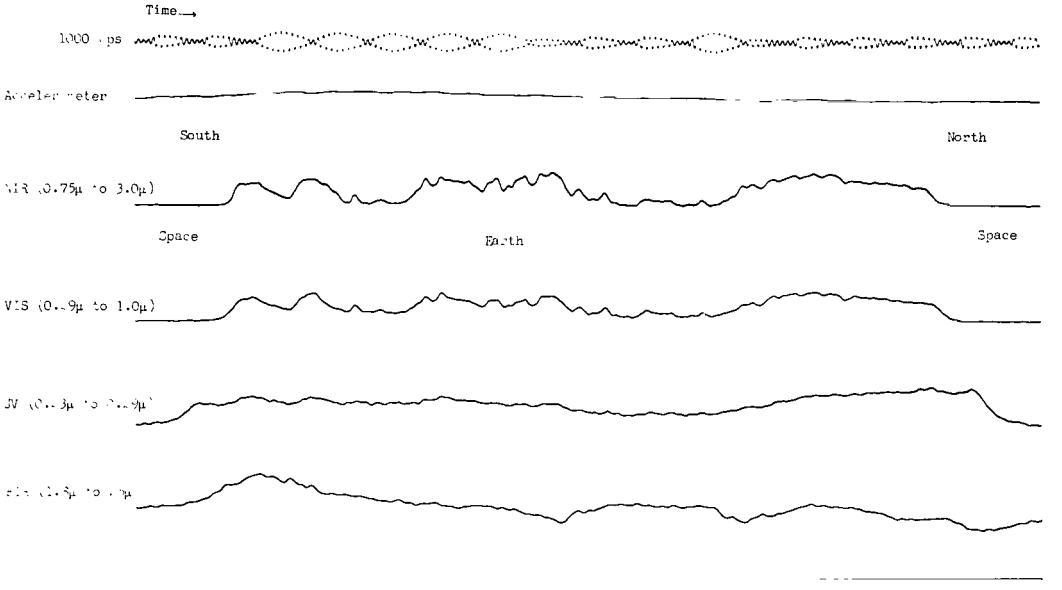

(b) First sample for vehicle altitude of 450 km.

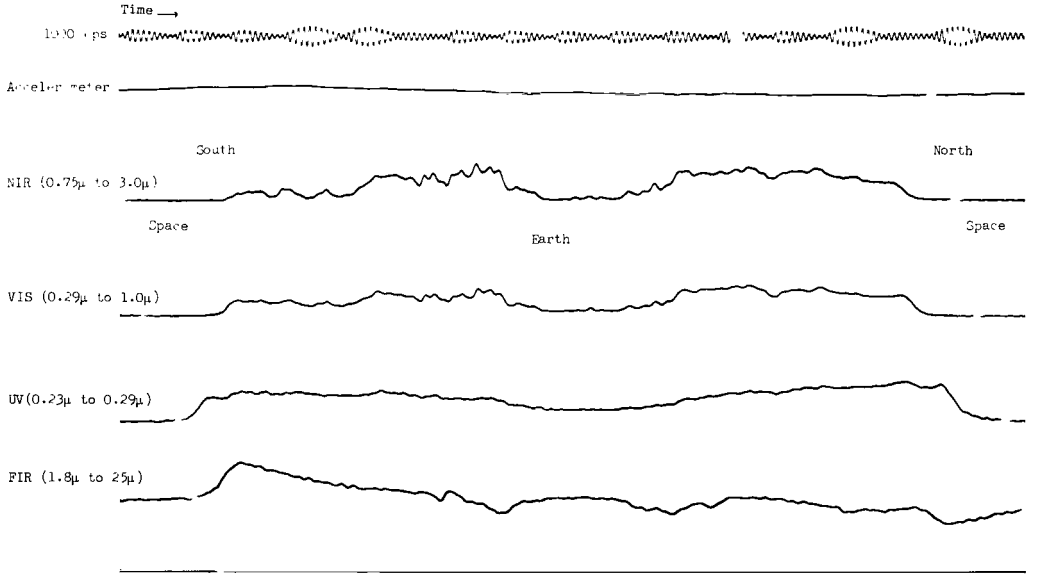

(c) Second sample for vehicle altitude of 450 km.

Figure 13.- Continued.

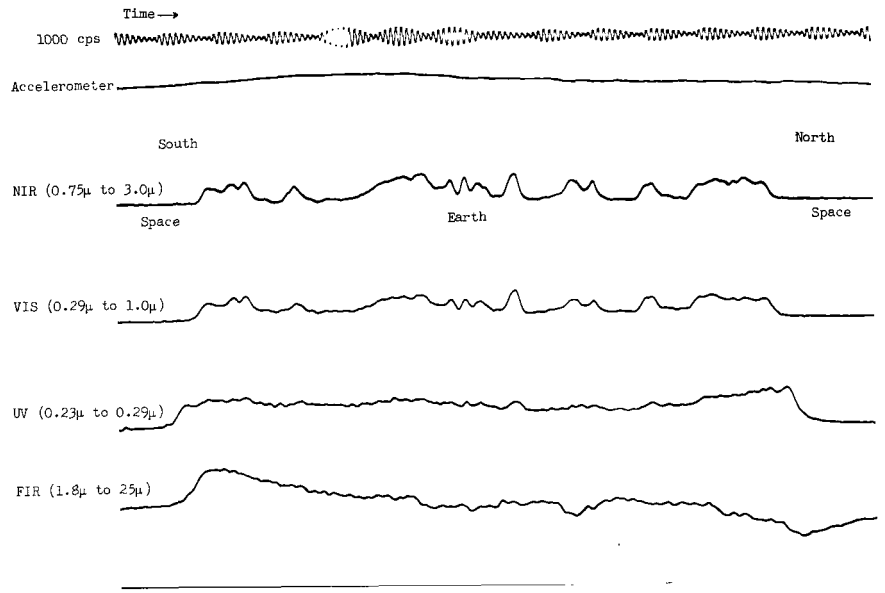

(d) First sample for vehicle altitude of 600 km.

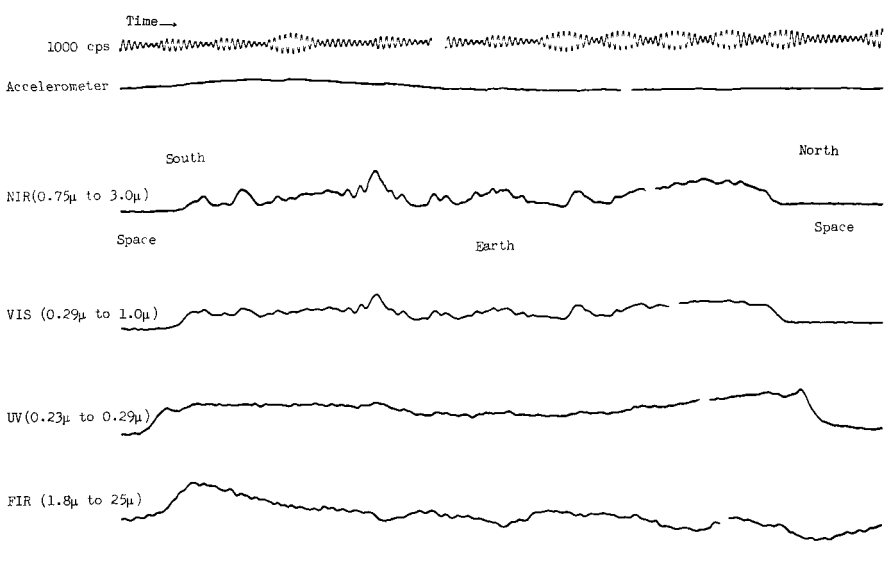

(e) Second sample for vehicle altitude of 600 km.

Figure 13.- Concluded.

All the horizon gradients, except the FIR northern horizon gradient which is always poorly defined, were well defined in figures 13(b) and (d). Figures 13(c) and (e) show that the NIR southern horizon lacks the definition previously noted. In figure 13(d), the signal rises out of the noise level and settles back into the noise level quite rapidly in the VIS and NIR channels, whereas the UV channel indicates a gradual rise. Figure 13(a) shows the gradual return of the northern gradient to a space reference in the UV channel quite well. This gradual return could indicate a possible high atmospheric effect.

From an initial view of the data it was evident that each scan would nearly repeat itself every 13 or 14 roll cycles. This fact, plus the knowledge that spinning bodies precess, indicated that the vehicle completed between 13 and 14 rotations per precession cycle. For purposes of data reduction 7 precession cycles, consisting of 13 scanning cycles each, was chosen. The altitude difference between precession cycles was approximately 50 km and data sampling started at nearly 300 km.

Two areas of importance to the study of horizon definition that are not presented herein are the position of the gradients with respect to the solid earth and an altitude measure of the duration of the gradients. These results are not available at this time.

Horizons

Horizon data are presented in figures 14 to 17. The radiances for the VIS and FIR horizons are given in figures 15 and 17. Only relative radiances are given for the NIR horizon (fig. 14) and UV horizon (fig. 16) since problems have arisen which indicate possible errors in the calibration of these channels. The magnitudes of the relative radiance scales in figures 14 and 16 are arbitrary. Figure 14 shows the distribution of relative radiances of the NIR southern and northern horizons.

Since scattering produces no termination of the horizon prior to cloud levels in the NIR, the variation of relative radiance by a factor of more than 4 in the southern horizon could have been caused by irregular cloud cover.

A ratio of the southern mean to the northern mean of the measured data is 0.58 whereas the ratio of the calculated radiances at 5 km is 0.59 (fig. 6). This ratio is important because it is produced by the position of the sun which affects the scattering angle in Rayleigh scattering. There is no reason for sunlight reflected from clouds or the earth to have a similar sensitivity to solar position; so the agreement of the ratio of the southern to northern horizon mean values with theory along with the large standard deviations leads one to conclude that scattering is important in the horizon formation but clouds cause large variations. The point at which the horizon gradient terminated is sometimes difficult to determine in the NIR. Figure 13(a) shows a very clean NIR southern horizon gradient, but figure 13(e) shows an instance where a small plateau occurred and then the signal increased to a peak. The beginning of the plateau was read as the termination of the gradient. In general, the first major slope change after the basic slope of the profile was established is

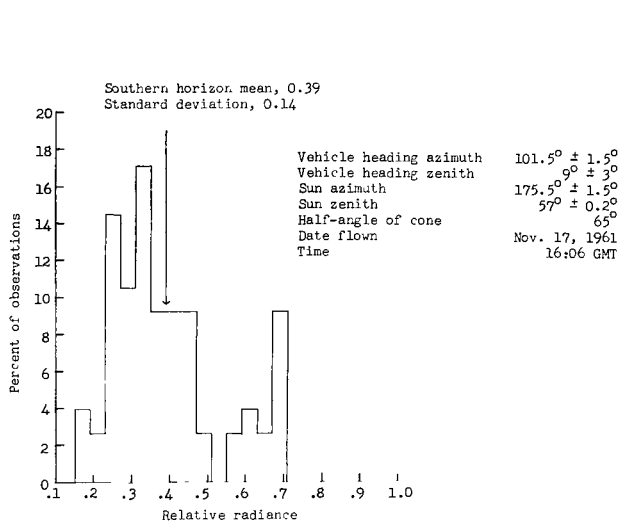

(a) Southern horizon.

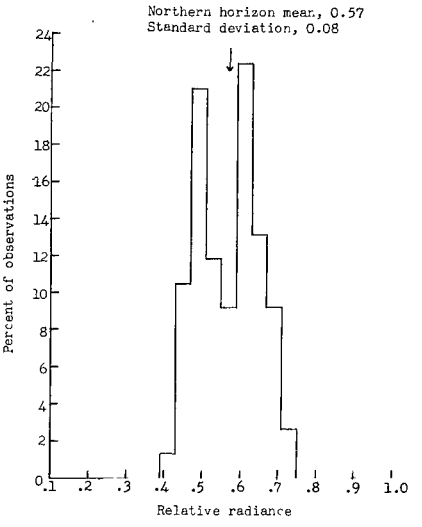

(b) Northern horizon.

Figure 14.- Distribution of relative radiances observed for NIR (0.75μ to 3.0μ).

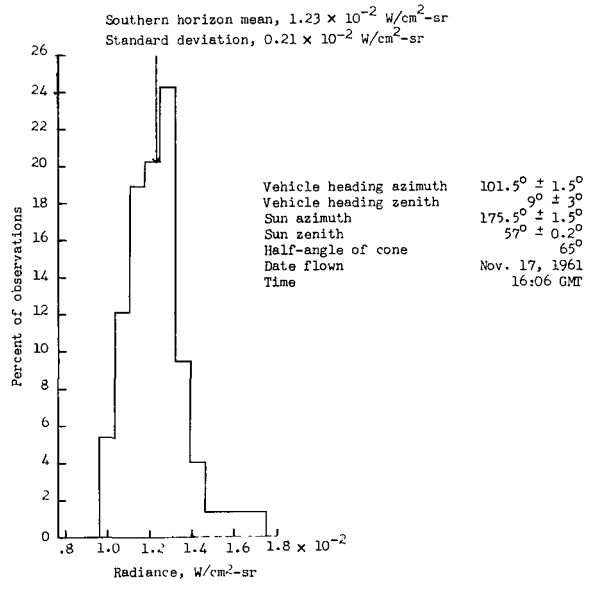

(a) Southern horizon.

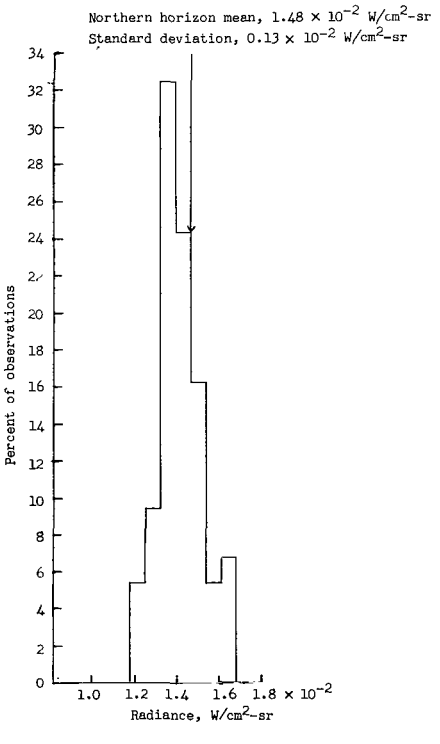

(b) Northern horizon.

Figure 15.- Distribution of radiances observed for VIS (0.29μ to 1.0μ).

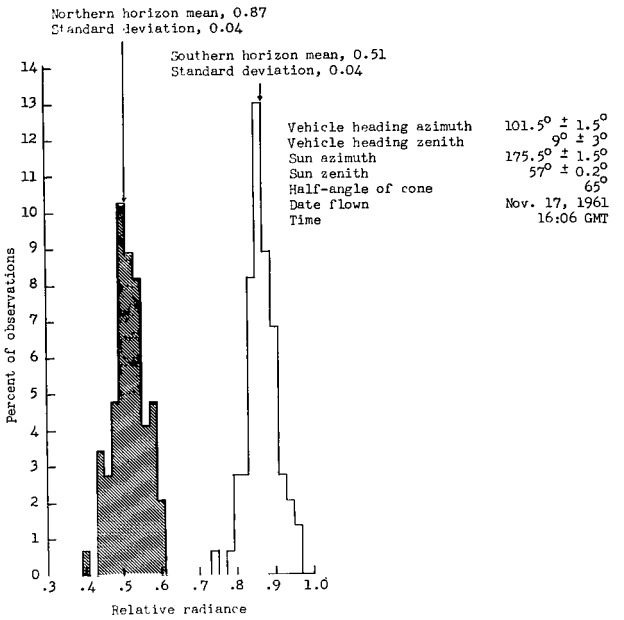

Figure 16.- Distribution of relative radiances observed for UV (0.23μ to 0.29μ) northern and southern horizon.

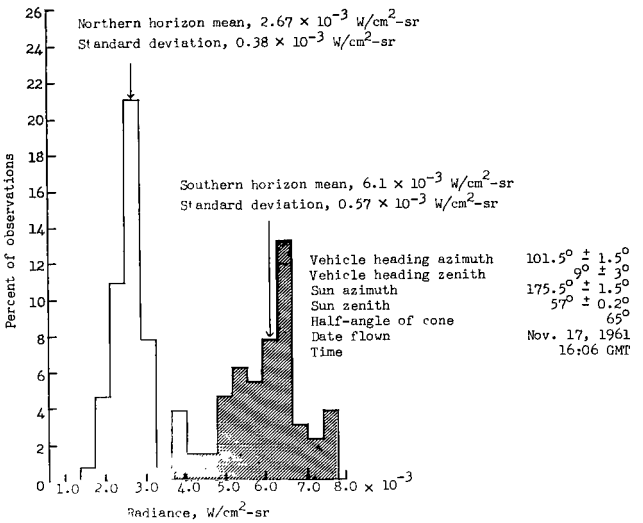

Figure 17.- Distribution of radiances observed for FIR (1.8μ to 25μ) northern and southern horizon.

interpreted as the termination of the horizon gradient. With the large variations of the relative radiances observed the NIR spectral band is a poor one to use for horizon definition. This conclusion does not exclude the possibility of an NIR airglow horizon above the one measured here since a greater sensitivity is necessary for such a measurement.

Radiances of the southern and northern horizons in the VIS channel are shown in figures 15(a) and (b). The spread in radiances observed is less than a factor of 2, and the values for the northern and southern horizons are nearly the same. The mean radiance for the southern horizon is 1.23×10^{-2} W/cm^2-sr and the theoretical radiance from figure 5 is 1.30×10^{-2} W/cm^2-sr. For the northern horizon the mean radiance is 1.48×10^{-2} W/cm^2-sr and the theoretical radiance from figure 5 is 1.75×10^{-2} W/cm^2-sr. A radiance of 1.48×10^{-2} W/cm^2-sr is comparable to a diffuse reflection of 46 percent which is quite reasonable for certain clouds. The maximum error for an individual measurement is estimated to be ±30 percent. Notice that the mean radiance for the northern horizon is slightly higher than that for the southern horizon as predicted by primary scattering. The ratio of the southern mean to the northern mean is 0.83, whereas primary scattering predicts 0.75. The standard deviations when compared to the mean radiances are smaller for the VIS than for the NIR, and the extremes of radiances observed are also smaller than for the NIR. In addition the VIS horizon is at a slightly higher altitude than the NIR horizon as seen in figure 13. All these facts lead to the conclusion that the VIS horizon was principally caused by scattering even though reflections from clouds could yield comparable radiance levels. If the horizon peak radiance is taken

to be about 10 km (as predicted in fig. 5), then clouds could definitely affect a measurement of this type.

The UV relative radiances (fig. 16) for the northern and southern horizons are definitely different. The fact that the relative radiance of the northern horizon is larger than that of the southern horizon is predicted by primary scattering theory. (See fig. 4.) This difference is due to the orientation of the radiometer with respect to the sun and earth. The ratio of the southern peak to the northern peak is 0.63 for calculations and 0.59 for the measured data. The relatively small variation of relative radiance at both northern and southern horizons indicated a stable condition. The vertical distribution of ozone plays a role in determining the magnitude and altitude location of the profile, and it is known that the distribution of ozone varies with time and geographical location. The peak of the UV horizon profile is the most obvious feature of any horizon gradients measured.

The FIR radiances (fig. 17) from the northern and southern horizons are significantly separated but, in contrast with the UV, the FIR southern horizon has a higher radiance than the northern horizon. Since a temperature can be associated with the FIR horizons, the southern horizon is warmer than the northern horizon. As a comparison the mean radiance of 6.1×10^{-3} W/cm^2-sr of the southern horizon is equivalent to 257° K; likewise, the mean radiance of 2.67×10^{-3} W/cm^2-sr of the northern horizon is equivalent to 215° K. Standard deviations of 0.57×10^{-5} W/cm^2-sr and 0.38×10^{-3} W/cm^2-sr for the southern and northern horizons correspond to 5° K and 6° K. The maximum error for an individual radiance measurement is estimated to be ±30 percent. Theoretical computations of horizon gradients in reference 10 indicate effective temperatures in this same range. The temperature extremes measured were 270° K for the southern horizon and 205° K for the northern horizon. Since the difference in radiances for the northern and southern horizons is interpreted as a temperature difference, this spectral band should have horizons dependent on meteorological conditions which might make it a poor band for horizon definition.

CONCLUDING REMARKS

Measurements of the sunlit horizons of the earth were made in the four spectral bands: 0.23μ to 0.29μ, middle ultraviolet (UV); 0.29μ to 1.0μ, visible (VIS); 0.75μ to 3.0μ, near infrared (NIR); and 1.8μ to 25μ, far infrared (FIR). The four-channel radiometer was flown on a Javelin vehicle from NASA Wallops Station.

Theoretical considerations indicate that the NIR region would be radically affected by local weather conditions since the altitude of the horizon peak radiance is low enough to make the reflection of clouds change the measured radiances. The factor-of-four variation in the measured relative radiances of the NIR region tends to substantiate the fact that local meteorological conditions determine the horizon; therefore, the predictability of the horizon in this region would be poor.

In the VIS region the horizons predicted by primary scattering occur at an altitude where they could be affected by the relatively high clouds occurring above an altitude of 10 km. The radiances predicted by primary Rayleigh scattering in the VIS region agree quite well with the measured radiances but both these fall in a region where the energy could also come from cloud reflections. The altitude of the VIS horizon was greater than that of the NIR horizon and because the measured radiances varied by a factor of 2 in the VIS region instead of by a factor of 4 as in the NIR region, it is believed that clouds affect the VIS horizon less than the NIR region; thus, primary scattering is more important in the VIS band than in the NIR band.

The theoretical horizon in the UV band depends upon the ozone distribution, and for a typical distribution the peak radiance of the horizon profile occurs at 58 km, well above cloud altitudes. The measured radiance peaks in the UV occurred well above either the NIR horizon or the VIS horizon and evidence indicates that this was a scattering peak even though no determination of the actual radiances could be made. With more information about the ozone content of the atmosphere and its distribution, the sunlit UV horizon could be a predictable and possibly a relatively stable horizon.

A definite radiance and hence temperature difference existed between the northern and southern horizons in the FIR spectral region. Effective blackbody temperatures ranging from 205° K to 270° K were probably caused by cloud distributions and vertical temperature structure which indicates that the horizon profile in this FIR band is difficult to predict and subject to large changes.

Langley Research Center,
National Aeronautics and Space Administration,
Langley Station, Hampton, Va., August 27, 1964.

REFERENCES

1. McKee, Thomas B.: Rocket Observations of the Earth's Limb. M.A. Thesis, The College of William and Mary in Virginia, Aug. 1963.

2. Anon.: Handbook of Geophysics. Revised ed., The Macmillan Co., 1961.

3. Coulson, Kinsell L.: The Flux of Radiation From the Top of a Rayleigh Atmosphere. Sci. Rept. No. 1 (AFCRC TN 59 402, ASTIA AD 216 317), Dept. Meteorology, Univ. of California at Los Angeles, Jan. 1959.

4. Elsasser, Walter M.; and Culbertson, Margaret F.: Atmospheric Radiation Tables. AFCRL-TR-60-236, Dept. Phys., Univ. of California, [1960].

5. Chamberlain, Joseph W.: Physics of the Aurora and Airglow. Academic Press, Inc., 1961.

6. Noxon, J. F.; and Goody, R. M.: Observation of Day Airglow Emission. J. Atmospheric Sci. (Notes and Correspondence), vol. 19, July 1962, pp. 342-343.

7. Friedman, Herbert: A Survey of NRL Research Results Obtained Since the Last COSPAR Meeting. Space Research II, H. C. van de Hulst, C. deJager, and A. F. Moore, eds., Interscience Publ., Inc., 1961, pp. 1021-1035.

8. Hrasky, William C.; and McKee, Thomas B.: Radiance of the Earth and Its Limb in the Middle Ultraviolet. NASA TN D-2355, 1964.

9. Friedman, R. M.; Rawcliffe, R. D.; and Meloy, G. E.: Radiance of the Upper Atmosphere in the Middle Ultraviolet. Rept. No. TDR-169(3260-50) TN-4 (SSD-TDR-63-162), Aerospace Corp. (El Segundo, Calif.), July 26, 1963.

10. Hanel, R. A.; Bandeen, W. R.; and Conrath, B. J.: The Infrared Horizon at the Planet Earth. J. Atmospheric Sci., vol. 20, no. 2, Mar. 1963, pp. 73-86.

11. Burn, James W.: The Application of the Spectral and Spatial Characteristics of the Earth's Infrared Horizon to Horizon Scanners. IEEE, Trans. Aerospace, vol. AS-1, no. 2, Aug. 1963, pp. 1115-1126.

12. Childs, Charles B.: Broad-Band Ultraviolet Filters. NASA TN D-697, 1961.

13. Nicodemus, Fred E.; and Zissis, George J.: Methods of Radiometric Calibration. 4613-20-R (Contract SD-91), Inst. Sci. Technol., Univ. of Michigan, Oct. 1962.

"The aeronautical and space activities of the United States shall be conducted so as to contribute . . . to the expansion of human knowledge of phenomena in the atmosphere and space. The Administration shall provide for the widest practicable and appropriate dissemination of information concerning its activities and the results thereof."

—NATIONAL AERONAUTICS AND SPACE ACT OF 1958

NASA SCIENTIFIC AND TECHNICAL PUBLICATIONS

TECHNICAL REPORTS: Scientific and technical information considered important, complete, and a lasting contribution to existing knowledge.

TECHNICAL NOTES: Information less broad in scope but nevertheless of importance as a contribution to existing knowledge.

TECHNICAL MEMORANDUMS: Information receiving limited distribution because of preliminary data, security classification, or other reasons.

CONTRACTOR REPORTS: Technical information generated in connection with a NASA contract or grant and released under NASA auspices.

TECHNICAL TRANSLATIONS: Information published in a foreign language considered to merit NASA distribution in English.

TECHNICAL REPRINTS: Information derived from NASA activities and initially published in the form of journal articles.

SPECIAL PUBLICATIONS: Information derived from or of value to NASA activities but not necessarily reporting the results of individual NASA-programmed scientific efforts. Publications include conference proceedings, monographs, data compilations, handbooks, sourcebooks, and special bibliographies.

Details on the availability of these publications may be obtained from:

SCIENTIFIC AND TECHNICAL INFORMATION DIVISION

NATIONAL AERONAUTICS AND SPACE ADMINISTRATION

Washington, D.C. 20546